Fatigue Crack Growth Mechanisms of Two Titanium Alloys at Room and Elevated Temperatures

Y. Dai*, N. Marchand*, M. Hongoh** and J. I. Dickson*

*Dept. of Metallurgical Engng.
Ecole Polytechnique de Montreal
Canada H3C 3A7

**Pratt & Whitney Canada
LONGUEUIL (Quebec)
Canada J4G 1A1

ABSTRACT

Fatigue crack growth mechanisms at room and elevated temperatures of two titanium alloys, respectively Ti-6Al-4V and Ti-6Al-2Sn-4Zr-6Mo, were studied. Single edge notched specimens, which were fabricated from turbine compressor discs forgings, were used in this study. Crack initiation and crack growth rates (da/dN) for both small and long cracks emanating from the root of the notch were monitored using an advanced Alternating Current Potential Drop (ACPD) technique. The da/dN were plotted as a function of the stress intensity factors (ΔK_I) which were computed using respective short and long crack solutions. Correlation of da/dN data with ΔK_I suggest that fatigue crack growth is controlled by ΔK_I soon after nucleation ($a > 60\mu m$). The microscopic features of the fractured surfaces at different stages of fatigue crack growth are observed and analyzed. The results showed that the relationship between the crack front and the α/β interface controls the materials' resistance to fatigue crack growth.

1. INTRODUCTION

Titanium alloy forgings are extensively used in gas turbine engines for applications ranging from impellers, compressor discs and blades to sealings, cases and fan blades just to name a few. In recent years, the demand toward achieving higher thrust-to-weight ratios has led to increasing the temperatures of most stages (compressor, combustion and turbine) of the engines. As a result of operating at higher temperatures, compounded by the introduction of new regulations for safety, the accurate predictions of the low cycle fatigue life (i.e. the fatigue crack initiation life to 1/32" surface crack) as well as of the crack propagating lives (da/dN) has become paramount for Ti-based components. Furthermore, the accurate quantifications of the fatigue behaviour under realistic operating conditions including thermal-mechanical fatigue conditions must now taken into account in all the design stage of the components(1-2).

Fatigue cracks in a compressor disc usually start where some form of geometrical discontinuity exists such as fir tree root, slots and bolt holes. Recent advances in crack detection techniques such as ACPD techniques has rendered possible the detailed monitoring of crack initiation and growth mechanisms using laboratory specimen with notch features identical to those

Titanium '92
Science and Technology
Edited by F.H. Froes and I. Caplan
The Minerals, Metals & Materials Society, 1993

encountered in engine components(1,3). However, the study of cracks initiating from notches requires that 1) cracks with lengths (or depths) as small as 40μm be detected and their subsequent growth monitored with equal accuracy (Δa ~ 1-2 μm), 2) the critical crack length for which further growth is mostly controlled by fracture mechanics must be determined, and 3) the proper stress intensity factors (ΔK)'s) that take account the stress field of the notch must be used when correlating the da/dN data.

Several mechanisms of fatigue crack initiation in $\alpha+\beta$ titanium alloys have been studied (3-5), including α/β interface cracking, primary α cracking at slip bands or slipless cracking, subsurface cracking by a cleavage-type, and grain egression. In addition to effects of microstructure, the operative mechanisms of crack initiation is also affected by a variety of mechanical and environmental conditions such as frequency of loading, R_ratio, temperature and corrosive environment.

2. MATERIALS AND EXPERIMENTAL PROCEDURES

Two titanium alloys were tested, both were fabricated from turbine compressor disc forgings. The microstructure of an α-ß forged Ti64 forging is shown in Figure 1. It can be seen that the equiaxed α particles, with average size about 32μm, are distributed in a transformed $\alpha+\beta$ matrix. The microstructure of an ß forged Ti6246 forging is also shown in Figure 1. The structure is featured by a coarse, acicular α-phase in the transformed ß phase. The average α lath size is about 2 X 60μm. Both alloys have volume fractions of α and ß phases of about 50%.

Composition analysis were performed using a JEOL 840 SEM with LINK spectrum analyzer. The chemical composition of beta stabilizers (V in Ti64 and Mo in Ti6246) varies from α to ß phases. These compositions were used as references to identify the fracture morphology associated with the different phases during the fractographic analysis.

The specimens used in this study were Single Edge Notched (SEN) specimens with rectangular cross section (W=10.67mm, B=5.33mm) and effective gauge length for extensometer equals to 25.4mm. A semi-circular notch (r/W = 0.1) was machined on the side of each specimen which matches the bolt hole geometries found in many engine compressor discs. The stress concentration factor (K_t) of the notch was found to be 2.12. The machining, cleaning and surface finishing procedures of the specimen were those that duplicate the actual manufacturing and conditions of the engine components. The tests were carried out under isothermal total strain controlled conditions using a high temperature extensometer attached to the back face of the specimen. Strain ranges investigated in this study varied between 0.2 ~ 0.4 % while the frequency was kept constant at 0.1667 Hz (10cpm). The specimens were heated using an induction heating system. The maximum temperatures for the tests were set at 400° C for Ti64 and 480°C for Ti6246.

The crack initiation and growth processes were monitored on-line using an advanced ACPD technique which has been described elsewhere(6). As compared with the Direct Current Potential Drop (DCPD) technique, the system sensitivity and linearity with respect to the measurement of crack length are enhanced by the skin effect which results from passing a high frequency AC current (30 KHz) through the specimen. Since the changes of potentials varied linearly with increasing crack length, the crack growth as a function of number of cycles was easily obtained from the ACPD curve which was continuously monitored during the test. With the present ACPD system, cracks as small as 20μm were detected with a probability of detection (POD) better than 95%. In turn, short and long crack growths (average) can be monitored

with an accuracy better than 2μm. Furthermore, the ACPD system was shown to be promising for studying the closure mechanisms for short and long cracks.

3. K_I SOLUTIONS

The stress intensity factor (K_I) for small cracks emanating from the notch root were calculated by a model proposed by J. Schijve(4). This solution uses the notch peak stress and is written as

$$K_I = C\ (t/r)\ \sigma_{pk}\ \sqrt{\pi t} \qquad (1)$$

Here σ_{pk} is the peak stress which is equal to $K_t\sigma_n$ with K_t the stress concentration factor and σ_n the far field nominal stress. C (t/r) is the notch geometry function which depends on t the crack depth measure from root surface and on r the radius of the notch. The function C(t/r) as derived by Schijve has the form

$$C(t/r) = 1.1215-3(t/r)+4(t/r)^{1.5}-1.7(t/r)^2 \qquad (2)$$

When the crack grows longer as compared to r, i.e when a/w >0.14 (see Figure 2), the K_I's were calculated using the equation derived by Marchand et al (9) for a SEN specimen under fixed-ends displacement conditions. This solution can be briefly written as

$$K_I = (N/BW)\ \sqrt{\pi a}\ H(\ \zeta,\ \eta,\ \eta_b\ ) \qquad (3)$$

Here N is the normal load *measured* during the test, B and W are the thickness and the width of the specimen, a is the crack length including the notch depth and $H(\zeta, \eta, \eta_b)$ is a geometrical correction factor which takes into account the actual loading conditions of the test (grips, no rotation ends, etc). For purpose of comparison, the K_I solution of Kujawaski(5) for a small notch crack in a semi-infinite domain was also used. When the cracks (a/W) are shorter than 0.14 (actual crack length t/W <0.04) the notch stress field controls the K_I's while for longer cracks the total crack length (notch plus actual crack length) and far field stress determine the K_I's. There exist a smooth transition between short and long crack solutions and thus a continuous solution for ΔK_I can be obtained to correlate the da/dN.

4. RESULTS

Crack Growth Kinetics

A typical fatige crack growth (FCG) rate vs. crack length curve for Ti64 tested at 400°C is shown in Figure 3. The following observations can be made from this figure. First, when the cracks are shorter (average depth from the root of the notch) than about 60μm, which is similar to the microstructural characteristic dimensions of the alloys, the da/dN varies erratically with increasing crack length, with da/dN spanning two orders of magnitude. This implies that these growth rates (for a<60μm) are (mostly) controlled by local microstructural events and thus are not and cannot be taken into account by a fracture mechanics parameter alone. When the crack grew longer than 60μm, their growth rates are well behaved (increased monotonically with increasing crack length) and thus can be correlated using a proper fracture mechanics parameter. Therefore it can be concluded that the da/dN's are controlled by fracture mechanics soon after initiation (a≥60 μm) for Ti64. The same conclusion was also found to hold for the Ti6246 forgings tested.

The da/dN - ΔK curve pertaining to results shown in Figure 3 is presented in Figure 4. In this plot, the short crack K-solution (i.e Eq.(1)) was used

for crack lengths ranging from 60 to 420μm while the long crack solution (i.e. Eq.(3)) was used for a > 420μm (a/W > 0.14, refer to Figure 2). For comparison, a set of long crack growth data is also plotted. Two conclusions can be drawn from this figure. Firstly, the da/dN for short cracks (60$\leq$a<130 μm) are faster than their long crack counterparts at the same level of ΔK. This is the result of the damage caused by inelastic deformation during cyclic straining. This was confirmed by carrying-out elasto-plastic finite element (FE) calculations which indicated the occurrence of small zones of inelastic deformation at the root of the notch. Secondly, as soon as the cracks grew outside the pre-damaged zone and into the elastic notch field (i.e 130 $\leq$a$\leq$ 420μm), the da/dN of the short crack became similar to that of the long cracks (at the same ΔK). This confirms that Schijive's K-solution takes properly into account the *elastic notch field*. Thus, short cracks emanating from notches can be considered as experiencing the following stages: (a) microstructural growth controlled, (b) inelastic damage growth controlled, (c) notch elastic field growth controlled, and (d) far-field stress growth controlled. As a result there exists three transitional (critical) crack lengths which are 60, 120 and 420μm for the Ti64 SEN tests. Similar results were also found for the Ti6246.

Fractographic observations

The Ti64 specimens tested at 400°C showed evidence of cleavage like facets morphology near the initiation sites at the root of the notch (see Figure 5a-5b). No cyclic cleavage striation was observed on these facets although fine and coarse fatigue striations were found near the cleaved facets. Compositional analyses showed these facets to be equiaxed α-phase particles, which is in agreement with other reported data (6-10). Analyses of sterofractographs of microregions at the initiation sites indicated that the crack nucleation planes coincide with the plane of maximum shear stresses obtained from the FEM results. Furthermore, see Figure 5c, analysis of several cleaved facets showed that fracture began near or at the α/β interface and proceeded toward the interior of the equiaxed α-phase particles. All this evidences suggest that the α-phase islands failed first and that the surrounding $\alpha+\beta$ matrix fractured under considerably higher cyclic strains as confirmed by the presence of coarse striations and faint cystallographic features in the $\alpha+\beta$ matrix. The above observations which pertains to the initiation zone were found to be more pronounced with increasing temperature. As expected, when the cracks grew outside the zone of influence of the notch, well defined fatigue striations are observed with secondary cracking occurring along the α/β interface and becoming more prevalent with increasing ΔK. For this region the measured microscopic da/dN are in agreement with those measured (bulk) by the ACPD technique. These results are also consistent with the observation of Rhodes et al.(7,9).

The fractured Ti6246 specimens also displayed numerous cleavage-like facets near the root of the notch, i.e. in the initiation zones (see Figure 6a). As expected, these facets were found to be the accicular α-phase grains. Subsurface cracking with clear cleavage-like facets were also observed in the 480°C tests. Due to the coarse microstructure of the material, the overall fractographic aspects of the surface appears relatively rougher as compared with Ti64. At moderate ΔK levels, but outside the zone of influence of the notch, delamination of acicular α-phase from the transformed β matrix is clearly visible (see Figure 6b). This indicates that crack growth proceeded through concurrent delamination of the α/β interfaces along the crack front. As a result, depending on the relative orientation of the α/β interfaces with respect to the loading axis, either striations along the delaminated areas (see Figure 6c) or secondary cracking along the α/β interfaces were produced. With increasing ΔK, interfacial secondary cracking

was promoted because it is the most efficient mechanism to reduce the actual stress field at the head of the main cracks. This is supported by the fact that secondary cracks coincide with the striations at high increasing ΔK level.

5. DISCUSSION AND CONCLUSIONS

Fatigue cracks initiation (FCI) at the primary α-phase is also consistent with the other reported initiation sites in (Al)-rich reqions (6). The (Al) contents for both alloys were found higher in the α than in the transformend β matrix. The crack initiation and growth at the $\alpha+\beta$ interfaces (especially observed in Ti6246 tests at 480°C) indicate that elongated preferentially oriented $\alpha+\beta$ interfaces (with respected to the notch) can be detrimental to the FCI and FCG resistance. As suggested by D. Eylon (10), the surface connected interfacial cracking is an indication of environmental effects on the fatigue crack initiation processes. Diffusion of oxygen (at elevated temperatures) from the surface into the material is enhanced along the α/β interfaces either by lattice mismatch between the hexagonal α and cubic β phases or by the interface stresses developed during the load cycles. Interfacial diffusion is also promoted by the higher surface to volume ratio associated with the acicular α-phase and higher dislocation density. The resulting higher interstitial contents embrittle the interface zone (11) and reduce its ability to plastic deformation.

From this study, the following conclusions can be made:

- The crack growth rates in Ti64 and Ti6246 are controlled by ΔK soon after initiation at root of the notch when a>60μm.
- Three transitional (critical) crack lengths were indentified for the notched specimens using the ACPD crack growth measurement technique. These critical crack lengths separate microstructural growth controlled, inelastic notch field growth controlled, elastic notch field growth controlled, and far-field stress growth controlled regions.
- The crack initiation sites for both alloy were found to be at the α-phase particles or α/β interfaces, with cleavage-like facet fractured morphology.
- The α/β interfacial cracking, assisted by high temperature environmental embrittlement controls the FCI and FCG resistance of Ti6246.

ACKNOWLEDGEMENT

This research is supported by the Canadian National Science and Engineering Research Council (NSERC) and Pratt & Whitney Canada under R&D project 661-001/89.

REFERENCES

1. N. J. Marchand, Y. Dai and M. Hongoh, P&WC, WY-910069, 102 pages, 1991.
2. Engine Structural Integrity Program (ENSIP), MIL-STD-1783, Nov. 1984.
3. Y. Dai, et al, Proc. of 5th Int. on LCF, Berlin, Sept. 1992, in press.
4. J. Schijve, Fract. of Engng. Mater. & Struc., Vol.5, pp.77-90, 1982.
5. D. Kujiawski, Fract. of Engng. Mater. & Struc., Vol.14, pp.953-965, 1991.
6. J. L. Gilbert and H. R. Piehler, Met. Trans. 20A, pp. 1715-1725, 1989.
7. C. G. Rhodes, Proc. of 4th Int. Conf. on Titanium, pp. 1701-1707, 1980.
8. J. C. Chesnutt, et. al, ASTM STP 600, pp. 99-138, 1976.
9. C. G. Rhodes and J.C. Williams, Met. Trans. 6A, pp. 1670-1671, 1975.
10. D. Eylon et al, 4th Int. Conf. on Titanium, pp. 1845-1854, 1980.
11. G. T. Gray III, et. al, Met. Trans. 21A, pp.95-105, 1990.

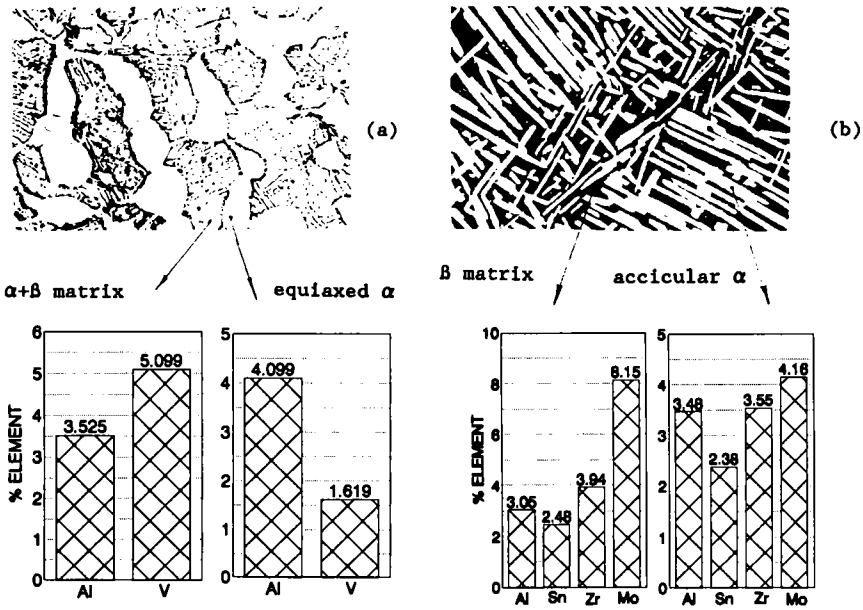

Fig.(1) Microstructure of the titanium forgings.
(a) Ti64, (b) Ti6246. (500X)

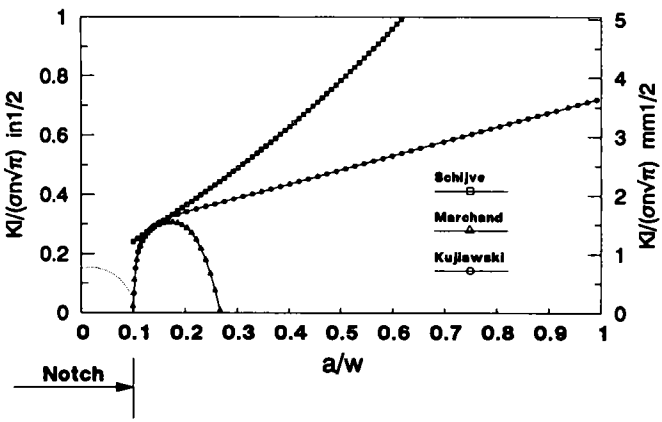

Fig.(2) K_I solutions for short and long cracks emanating at root of the notch.

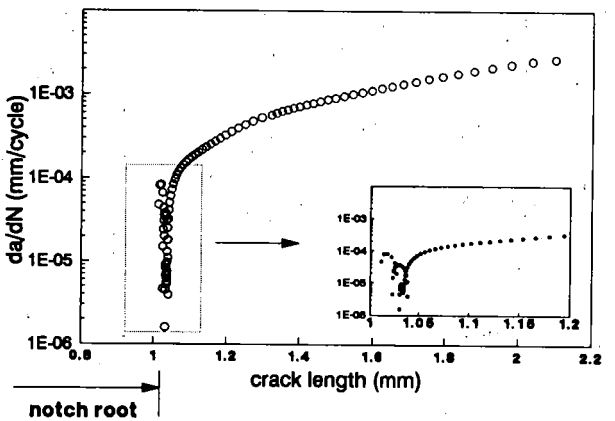

Fig.(3) A typical result for crack growth rate da/dN as a function of increasing crack length. Ti64 at 400°C.

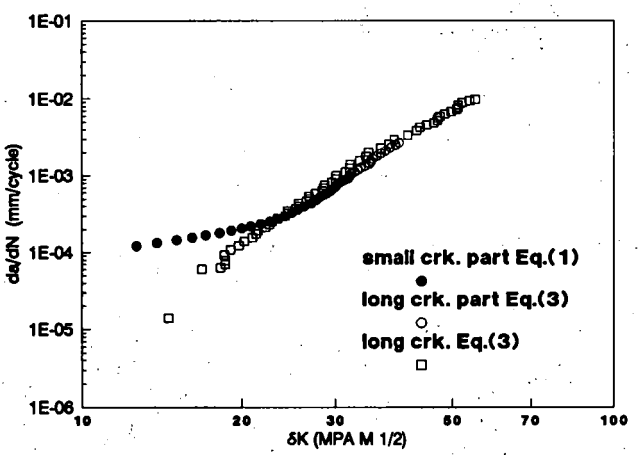

Fig.(4) Correlation of the da/dN data pertaining to Fig.(3) using ΔK computed for small and long cracks. Ti64 at 400°C.

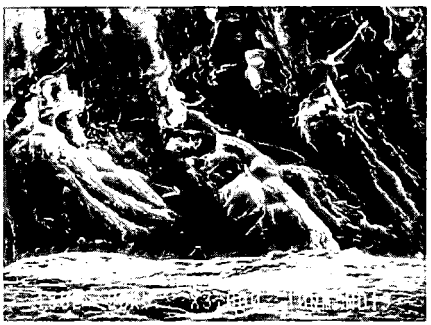

Fig.(5.a) Crack initiation site at root of the notch. Ti64, 400°C.

Fig.(5.b) Cleavage-like α facet at the Crack initiation site. Ti64, 400°C.

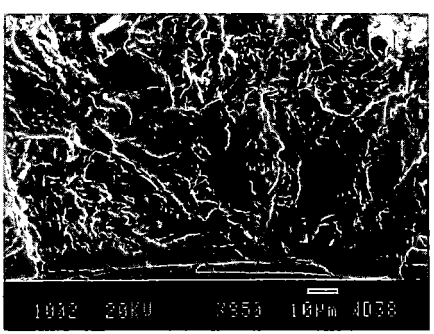

Fig.(5.c) Overview of the fracture surface near the notch. Ti64, 400°C.

Fig.(6.a) A initiation site at the root of the notch. Ti6246, 480°C.

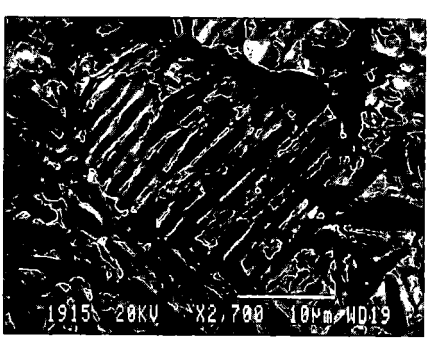

Fig.(6.b) Fatigue striations on the delaminated α-phases. Ti6246, 480°C.

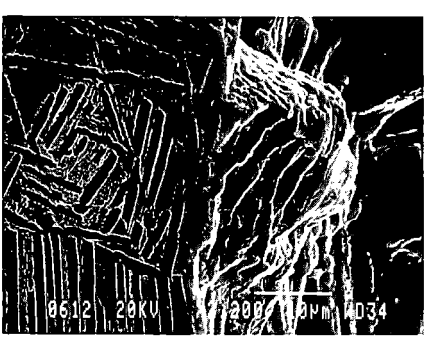

Fig.(6.c) Crack growth along the α/β interfaces. Ti6246, 480°C.